Well-Characterized Plasma Experiments for Validation of Computational Models

IEPC-2011-122

Presented at the 32nd International Electric Propulsion Conference,
Wiesbaden • Germany
September 11 – 15, 2011

Richard E. Wirz[1], Lauren Chu[2], Marlene Patino[2], Hann-Shin Mao[2], Samuel Araki[2]
University of California, Los Angeles, CA 90095

Abstract: UCLA researchers have developed a well-characterized plasma experiment that is designed to provide results for computational model development and validation. This effort supports the community's goal to develop computational engineering tools for predicting the performance and lifetime of existing and next generation electric propulsion devices. The experiment uses an ion beam and a precisely-defined "Test Cell" that can be pressurized to examine heavy species (i.e., ion and neutral) interactions. The Test Cell is a simple cylindrical experimental target domain that is well-suited for computational simulation. Currents are measured at electrodes surrounding the domain, as well as upstream and downstream of the domain. UCLA researchers are also developing a physics-based, multi-species hybrid-PIC model that provides insight into the dominant mechanisms within the Test Cell to aid in the design of the experiment. Comparison of the computational and experimental results show that the data follow expected trends at lower Test Cell pressures. At higher pressures, where the mean free path of the ions is less than the Test Cell length, the results do not agree as well. This disagreement is likely caused by the need to better treat multiple sequential ion-neutral collisions. Improvements to the experiment will provide higher spatial resolution and minimize uncertainty due to secondary electrons.

I. Introduction

Improved plasma models are necessary for the accurate simulation and characterization of advanced electric propulsion (EP) devices for space missions. In particular, behavior of partially-ionized plasma typical of electric propulsion devices is not well understood and accurate models in this regime are needed. Simple and well-defined experiments designed for validation of computational models are needed to facilitate systematic and confident development of plasma modeling capabilities. Such results will support efforts to develop engineering tools for computational design, performance evaluation, and lifetime prediction for existing and next generation EP thruster design and plasma processing systems. By examining fundamental physics and developing advanced modeling and simulation (M&S) capabilities, this effort also intends to establish fundamentals capabilities applicable to a wide range of plasma and propulsion concepts[1]. For example, the UCLA group is working with researchers at the University of Michigan to cater these results to code development and validation efforts for heavy plasma species using the Improved Concurrent Electromagnetic Particle-In-Cell (ICEPIC) model[2,3,4]. Some preliminary results using the data reported herein are given in references 4 and 5.

Previous researchers have provided many experiments that are well-suited to validating fully-developed codes for particular operating conditions[6,7,8,9,10,11]. These experiments are focused on describing particular mechanisms, such as cross-field diffusion; or measuring particle interactions, such as collision cross sections. In contrast, the

[1] Assistant Professor, Mechanical and Aerospace Engineering, 420 Westwood Plaza, Eng. IV 46-147B, wirz@ucla.edu.
[2] Graduate Student, Mechanical and Aerospace Engineering, 420 Westwood Plaza, Eng. IV 33-146.

focus of this research is to provide experimental results that are intended for the validation of computational models. Ideally and ultimately these experiments should:

- Provide simple and precisely-characterized results that include full disclosure of all relevant aspects of the experiment and measurements
- Allow isolation of important plasma mechanisms that are otherwise veiled by complicated experiments
- Facilitate systematic development and validation of plasma modeling capabilities

The main objective of the effort described in this paper is to provide well-characterized and simple experimental results for the validation of computational models for the behavior of heavy species (i.e., ions and neutrals). A secondary objective is to use a combined experimental and computational approach to understand the plasma dynamics within the experimental device to aid in the interpretation of the results and guide the future design of the experiment. Also, it is of interest to see to what extent existing plasmadynamic theory can be used to predict the results of this simple experiment.

II. Experimental Research Effort

A. Experimental Setup and Approach.

UCLA researchers have been developing an experimental facility to obtain detailed data for computational model validation for heavy species. To achieve this objective, the experiment uses a well-characterized ion beam facility (Figure 1) and a well-defined target domain, or "Test Cell'" (Figure 2) to provide precision measurements of plasma species currents in the presence of variable plasma conditions. The experimental facility is located at the Jet Propulsion Laboratory in Pasadena, California. Referring to Figure 1, Lens 1 and 2 are Einzel lenses, while the ExB filter serves as an energy filter. Apertures 1 and 2 are 5 mm in diameter. Deflection plate sets 1, 2, 4 are absolutely biased; that is, one plate is grounded. Deflection plate 3 is differentially biased horizontally and absolutely biased vertically. The deflection plates are used to steer the beam through the apertures and lenses of the facility. Additionally, the plates are used to steer the beam through a horizontal bend in the facility; this bend reduces the amount of neutrals from the Source Chamber that are seen in the Test Chamber.

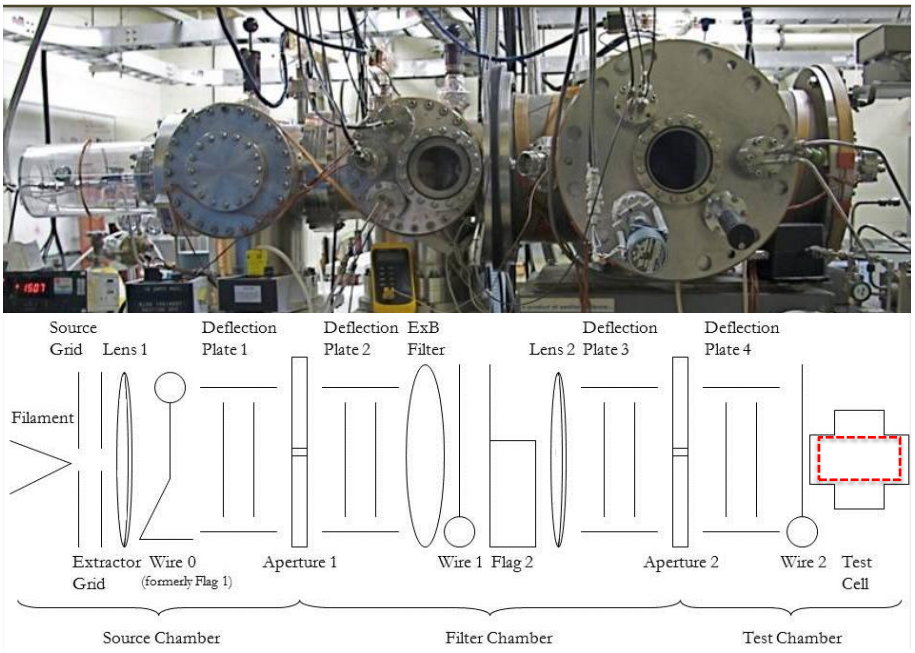

Figure 1. Ion Beam Facility with Test Cell (left-to-right: Source Chamber, Filter Chamber, and Test Chamber)

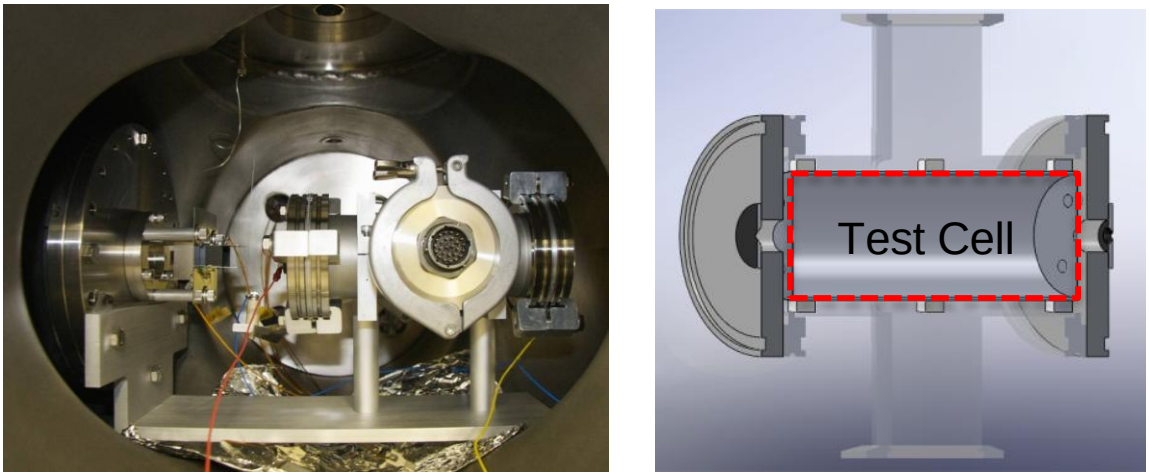

Figure 2. Well-defined "Test Cell" that serves as ion beam target. Left: Test Cell Installed in Test Chamber with ion beam entrance and deflection plates immediately before Test Cell. Right: Cut-away of Test Cell.

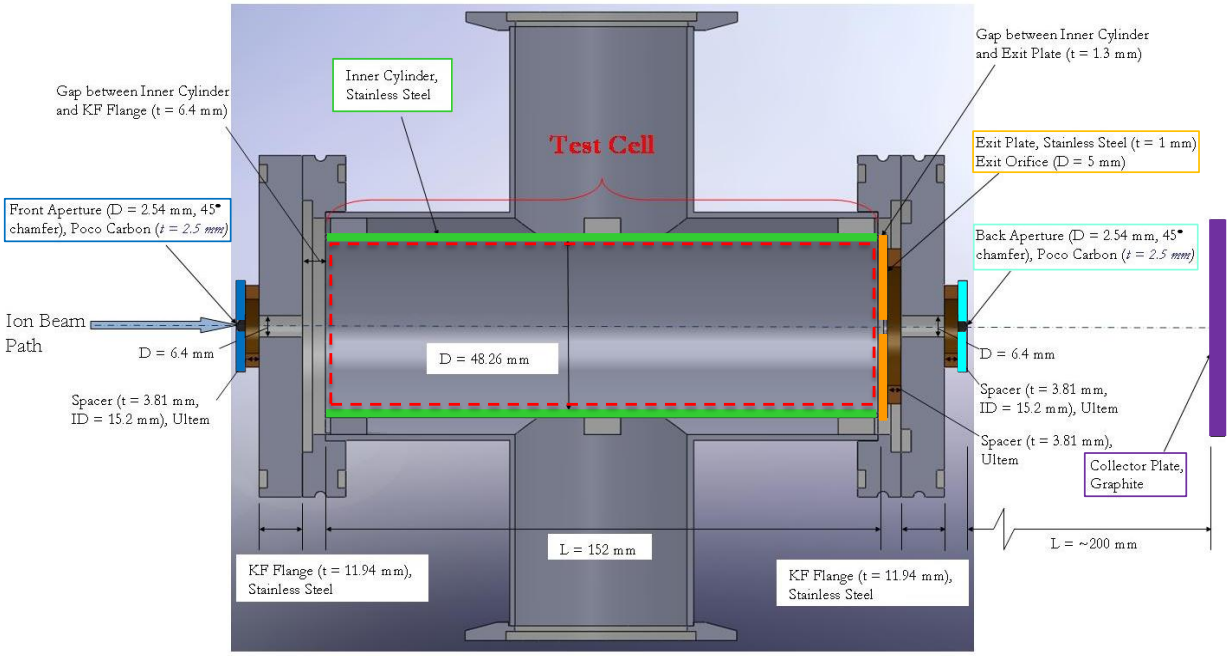

Figure 3. Schematic of Test Cell electrodes and important upstream and downstream electrodes.

As shown in Figure 3, the dimensions of the test cell and materials used for the electrode surfaces are well-defined; and the simple, axisymmetric Test Cell region is well suited for computational simulation. Materials that provide low secondary electron emission due to xenon impact, such as poco carbon and stainless steel, are used for the electrode surfaces.

Much of the early effort with the ion beam facility was focused on improving the beam scanning diagnostics to allow analysis at three distinct beam locations. These locations are designated by "Wire 0" just downstream of the ion source and the first lens, "Wire 1" just downstream of the ExB filter, and "Wire 2" which is 38 mm upstream of the Test Cell and 100 mm downstream of Aperture 2. Wire 0 is vertically scanned through the beam, while Wire 1 and 2 are both horizontally scanned. Additionally, Wire 0 is manually driven and Wire and 2 are motor driven.

Wire 0 is 0.635 mm in diameter while Wire 1 and 2 are 0.5 mm in diameter. All wires are tungsten. Profiles at Wire 2, upstream of the Test Cell, provide data for Test Cell input conditions for model development/validation efforts. For each data set, the Test Cell pressure is raised incrementally from base pressure of about 7.0×10^{-3} mTorr to several mTorr of xenon. At each pressure, a Wire 2 scan is taken to account for drift in ion beam input conditions.

To examine heavy species interactions, the xenon ion beam is held at constant conditions while the xenon neutral pressure inside the Test Cell is incrementally increased. The increase in Test Cell pressure causes an increasing number of beam ions that collide with neutral atoms via elastic and CEX collisions[12]. These collisions decrease the ion current that passes unimpeded through the cell and should increase the current to the electrodes that define the boundary of the Test Cell (i.e., the Inner Cylinder and the Exit Plate), as discussed later.

B. Experimental Results

For this paper, two data sets (Data Sets 1 and 2) are examined. The operating voltages for the ion beam used for these data sets are provided in Table 1. The Source Grid voltage determines the energy of beam ions. The Source and Extractor Grid and Lens 1 voltage values were chosen since they typically provide a well-behaved beam. During ion beam operation for a given day, the ion current to the collector plate is maximized by adjusting the deflection plate and lens voltages. Data Sets 1 and 2 were taken months apart with different filaments and, due to differences in the ion source conditions, different voltages were required for the maximum current condition. The beam scanning capabilities provided by Wires 0, 1, and 2 allow some understanding of beam evolution so that the beam can be analyzed at several locations along the ion beam facility. Figure 4 shows the beam profiles at Wire 0 and Wire 1 for Data Sets 1 and 2, where the ordinate axes express the current that is collected on the wire. These data show that the general profiles for the beam shape appears to be similar for each data set at the location of Wire 0 and 1. The integrated current for Data Sets 1 and 2 at Wire 0 are 3.63×10^{-6} and 3.70×10^{-6} A, respectively. The asymmetry of the Wire 1 scan is likely caused by the fact that Deflection Plates 1 and 2 are absolutely biased, as opposed to differentially biased, thus causing some scatter of the beam. The integrated currents for Data Sets 1 and 2 at Wire 1 are 1.42×10^{-7} and 1.52×10^{-7} A, respectively; revealing that about 95% of the beam is lost between Wires 0 and 1.

Table 1. Ion Beam Operating Conditions

Parameter	Data Set 1	Data Set 2
	Voltages (V)	Voltages (V)
Source Grid	1500	1500
Extractor Grid	1140	1140
Lens 1	-3000	-3000
Lens 2	-500	-1900
Deflection Plate 1 (Vertical, Horizontal)	(85, 143)	(86, 144)
Deflection Plate 2 (Vertical, Horizontal)	(-113, 149)	(-113, 152)
Deflection Plate 3 (Vertical, Left, Right)	(51.4, 148, 0.6)	(12.5, 146, -18)
Deflection Plate 4 (Vertical, Horizontal)	(-35.3, 9.4)	(-9.5, 22)

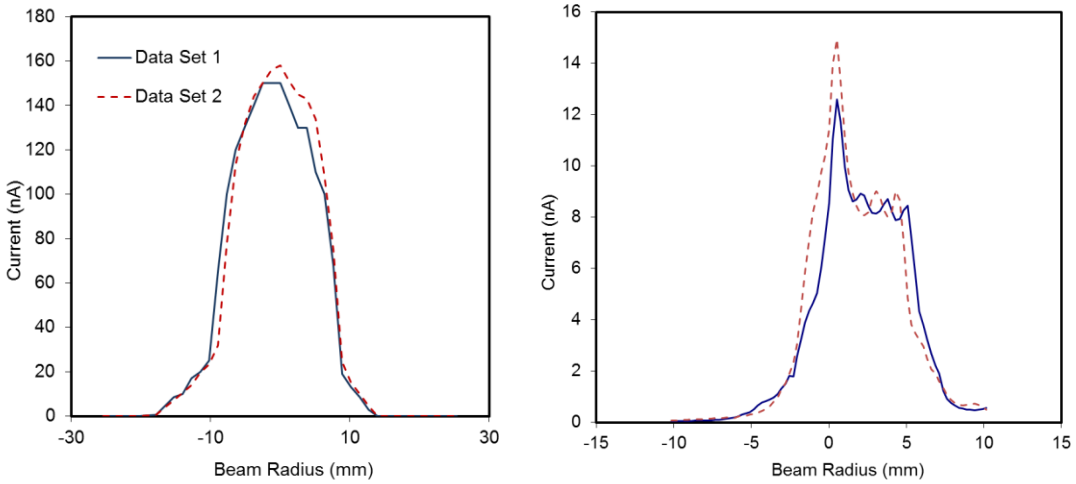

Figure 4. Wire 0 and Wire 1 beam profiles

Profiles at Wire 2, upstream of the Test Cell, provide data for Test Cell input conditions for model development/validation efforts. For each data set, the Test Cell pressure is raised incrementally from base pressure of about 7.0×10^{-3} mTorr to several mTorr of xenon. At each pressure, a Wire 2 scan is taken to account for drift in ion beam input conditions; this drift in the ion beam occurs primarily due to changes in cathode behavior and drift in the xenon feed rate into the discharge chamber of the ion source (the drift in feed rate is due to the fact that a needle valve is used for flow regulation into the Source Chamber, which is susceptible to thermal drift). In Figure 5, Wire 2 profiles for some Test Cell pressures are given; additionally, an average profile is shown surrounded by the envelope of maximum and minimum profile values. It should be noted that the change in the beam profile for each data set is predominately due to changes in source condition (i.e., cathode and source flow rate), regardless of changes in downstream conditions (i.e., Test Cell pressure), especially at lower Test Cell pressures. The integrated current for the average Wire 2 scans for Data Set 1 and 2 are 2.6×10^{-8} and 2.9×10^{-8} A, respectively; thus showing nearly an 80% loss in current between Wires 1 and 2.

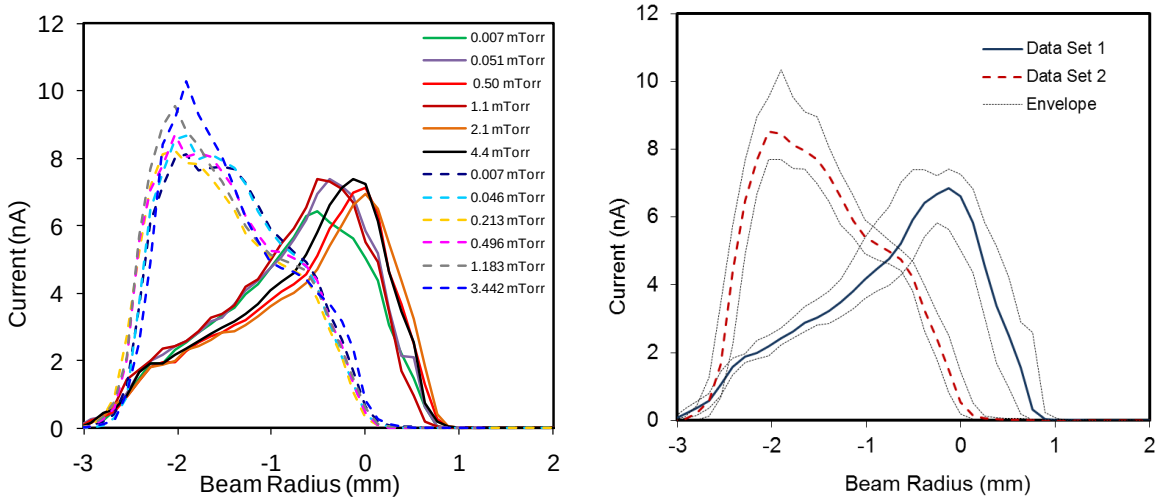

Figure 5. Wire 2 beam profiles. Note, on left figure, solid lines are for Data Set 1 while dashed lines are for Data Set 2.

Referring again to Figure 3, current is collected on an array of electrodes to develop a picture of the trajectories of the ions incident to the Test Cell. Figure 6 shows the normalized current collected on the Test Cell surfaces. The current values to the electrodes are normalized to the sum of the current that is measured to enter the Test Cell,

which is the sum of the current measured at the Inner Cylinder, Exit Plate, Back Aperture, and Collector Plate; thus excluding Front Aperture plate current. This sum also does not include the current that is deflected back through the upstream surface of the Test Cell region since there is not an electrode at that location. This electrode was not installed since these tests were originally intended for the low pressure regime where the mean free path is at least the length of the Test Cell and this surface was to be of minimal importance. The results show very good agreement between Data Sets 1 and 2, except the currents to the Back Aperture and Collector Plate show some disagreement. The larger current to the Back Aperture electrode for Data Set 2 suggests a larger beam divergence. Error bars for these measurements were derived from the percent error of the electrometers used to make the measurements.

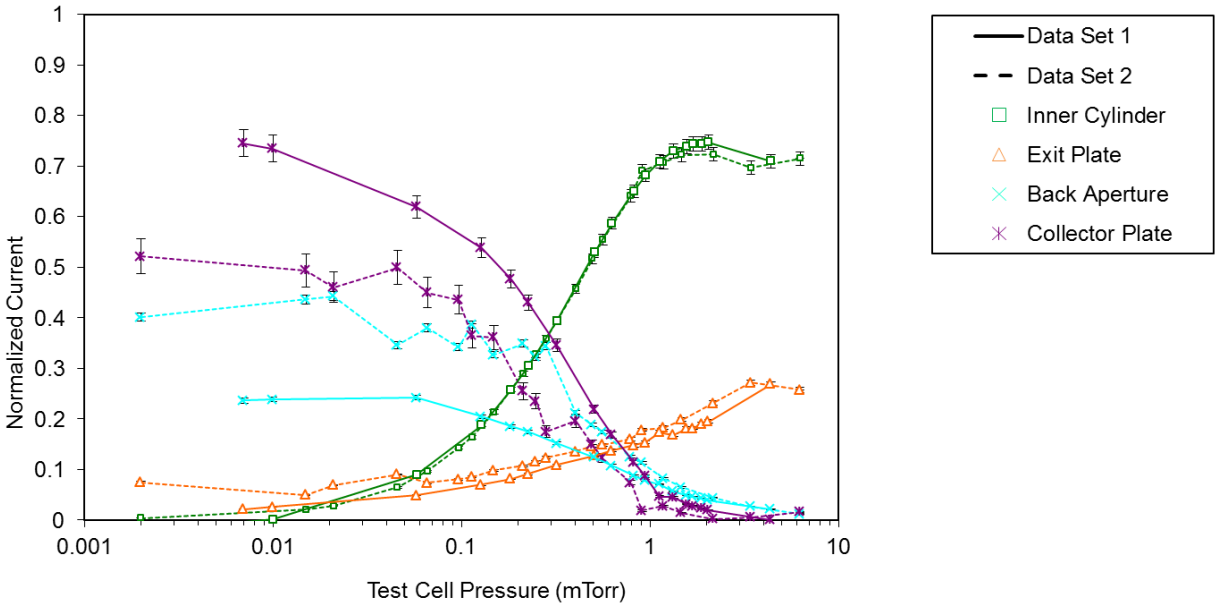

Figure 6. Normalized current to Test Cell electrodes and downstream of the Test Cell

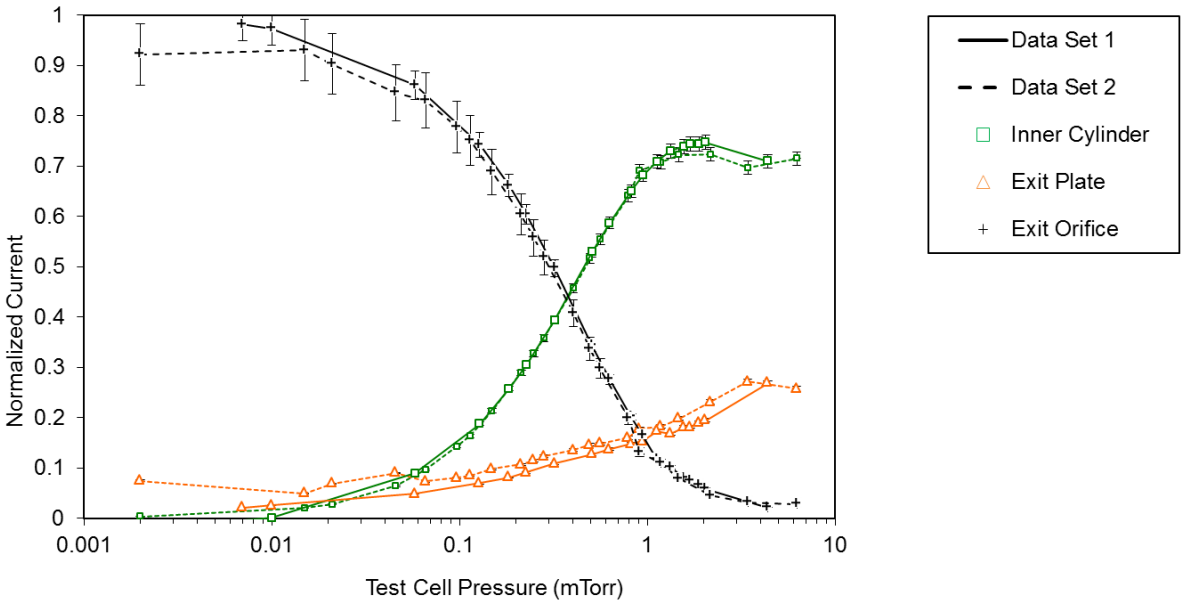

Figure 7. Normalized currents to Test Cell surfaces

To facilitate a discussion of the currents within the Test Cell, these data can be replotted to a form that gives a clearer picture of the behavior of the ions inside the Test Cell. Figure 7 expresses the current that passes through the Exit Orifice as the sum of the current collected at the Back Aperture plate and the Collector Plate. From this figure, it is clear that the current that passes through the Exit Orifice tend exponentially to zero with increasing pressure. As discussed in the next section, this exponential decrease is expected since the increasing pressure causes an increasing fraction of primary ions to experience elastic or CEX collisions before leaving the Test Cell. Similarly, the Inner Cylinder current is correspondingly increasing with increasing pressure due to the increased probability of collisions. The mechanisms responsible for this rise are discussed in the following section by comparing these results to a computational model. The Exit Plate experiences predominately monotonically increasing current with pressure, as expected; however, an eventual decrease at higher pressures is expected since the mean free path of the ions is less than approximately one-quarter of the Test Cell length at pressures above about 1.84 mTorr. Again, this behavior will be discussed in light of computational results in the following section.

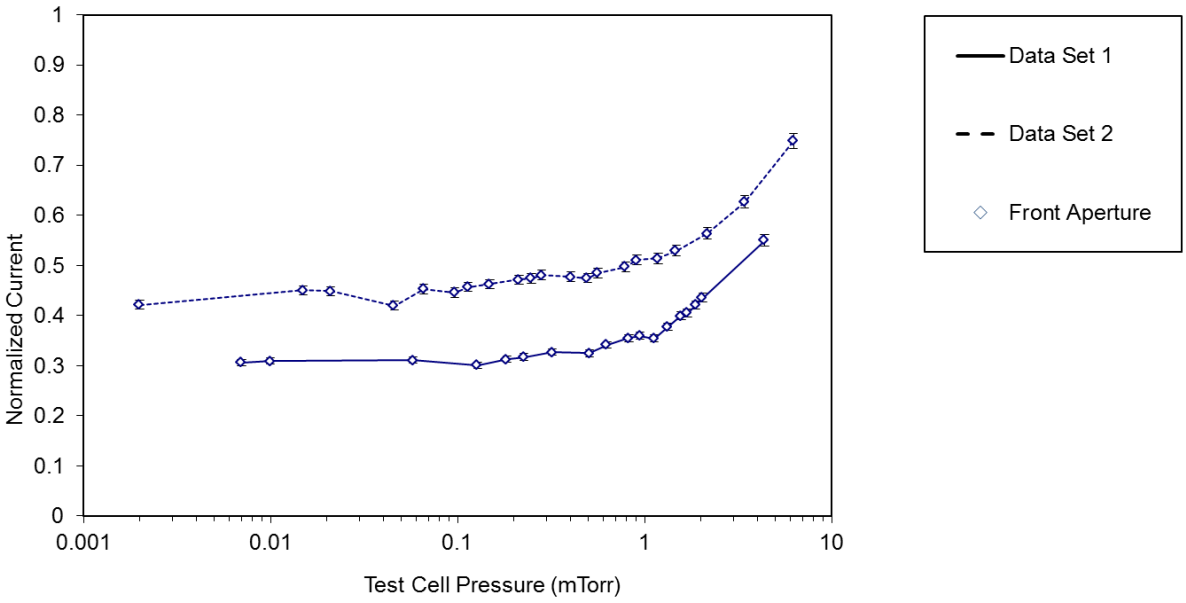

Figure 8. Normalized current to front aperture.

In Figure 8, the Front Aperture current is normalized to the sum of all Test Assembly currents, that is, the sum of the current measured at the Inner Cylinder, Exit Plate, Back Aperture, Collector Plate, and Front Aperture plate. From this plot, the Front Aperture plate current shows an increase with pressure, which suggests that an increased collisionality causes some spreading of the beam to the Front Aperture. This collisionality is likely due to the neutrals that are escaping the Test Assembly through the Front Aperture.

III. Computational Research Effort

A. Computational Approach

UCLA researchers are also developing a physics-based, multi-species hybrid-PIC model that provides insight into the dominant mechanisms within the Test Cell. The model uses a primary ion tracker, charge exchange (CEX) ion tracker, potential solver, fast neutral tracking, and secondary electron tracking. Details of the model are provided in Reference 5.

Miller et al.[6] provide a functional form of the cross section for Xe^+ + Xe symmetric charge exchange as a function of laboratory ion energy as

$$\sigma_i = [87.3 - 13.6\log(E)] \ \text{Å}^2$$

where σ_i includes the cross sections for both scattered primary and CEX ions, and E is the relative ion energy. For an ion energy of 1500V, σ_i is 44.1Å^2. Using this cross-section, the current depletion along the axis can be approximated analytically by

$$J(x) = J_0 e^{-n_o \sigma_i x}$$

where J and J_0 are the local and initial current values, n_o is the local neutral density, and x is the position along the axis.

B. Computational Results and Discussion

In this section, results from the computational model are compared to Data Set 1. This comparison allows the examination of the importance of primary and CEX ions to the currents measured in the Test Cell. This is done by showing results where just primary beam ions are considered (i.e., "Primary Only"), and then comparing to results where CEX ions created by collisions between the primary ions and the background neutral gas are also tracked to the electrodes (i.e., "Primary & CEX"). The model simulates the Test Cell domain assuming a uniform background gas and uniform density beam of 1500 V ions incident to the cell.

Initial trajectory results from the model (Figure 9) show representative trajectories of primary beam ions passing through the Test Cell for a neutral density of 10^{18} m^{-3}, corresponding to about 0.03 mTorr at room temperature. At this pressure, the mean free path of the ions is on the order of 2.27 m, thus most ions will pass through the Test Cell without experiencing a collision. These trajectories show that most primary ions do not experience a collision, while the ions that do collide with a neutral typically experience only one collision at this low pressure.

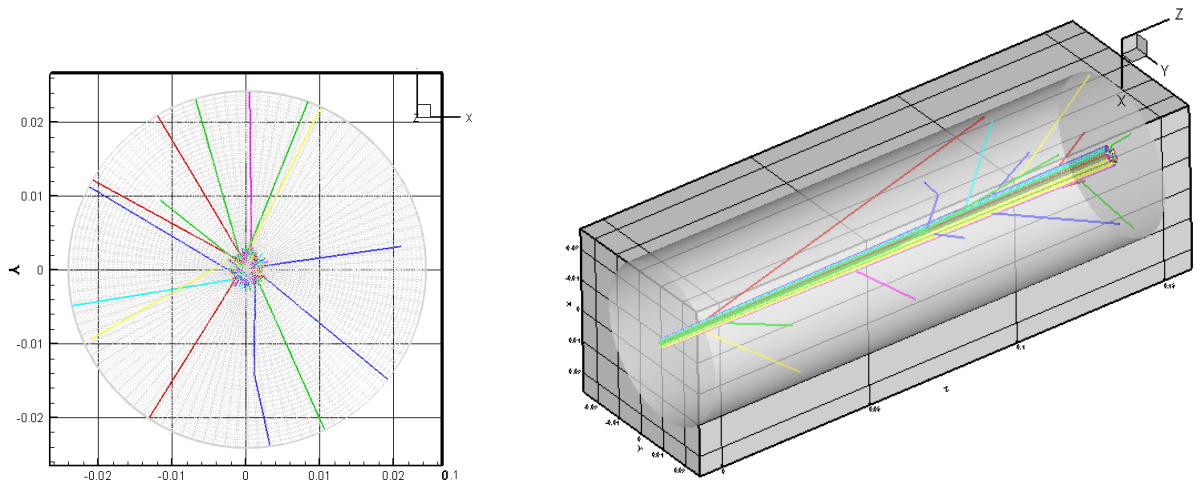

Figure 9. (Left) Particle trajectories looking along the test cell axis. (Right) Particle trajectories in 3D view. Particles are entering the Test Cell from the lower-left end of the cylinder

Figure 10 compares the analytical approximation of primary ion current depletion from the previous section to current that is measured to pass through the Exit Orifice during the experiment, and shows that the results agree fairly well. Similar agreement is obtained with the computational model. The relatively higher current predicted by the computational model is due to the fact that it accounts for small angle collisions events that will still result in primary ions passing through the Exit Orifice. The "Primary Only" and the "Primary & CEX" results are very close since the current that passes through the Exit Orifice is almost entirely primary ions.

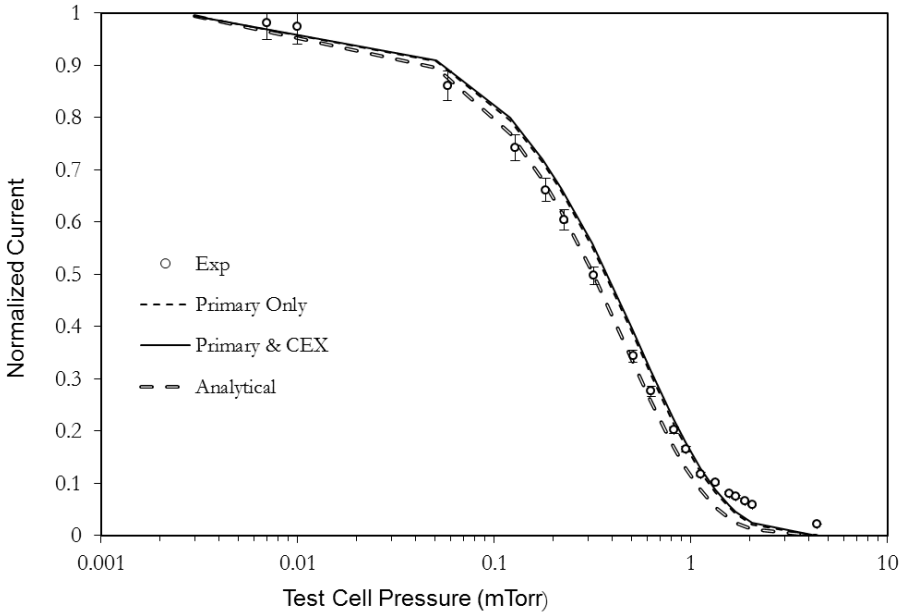

Figure 10. Comparison of experimental and computational results for current passing through the Exit Orifice.

Figure 11 plots the experimental and computational results for the Exit Plate. From this figure it is apparent that the computational model predicts that the majority of the current to the exit plate is due to primary ions. CEX ions are of importance near 0.5 mTorr where the mean free path is about the length of the Test Cell and it can be assumed that a sufficient population of CEX ions is created near the Exit Plate. The computational results suggest that the current to the Exit Plate should eventually fall due to increased Test Cell pressure; however, this trend is not seen in the experimental data.

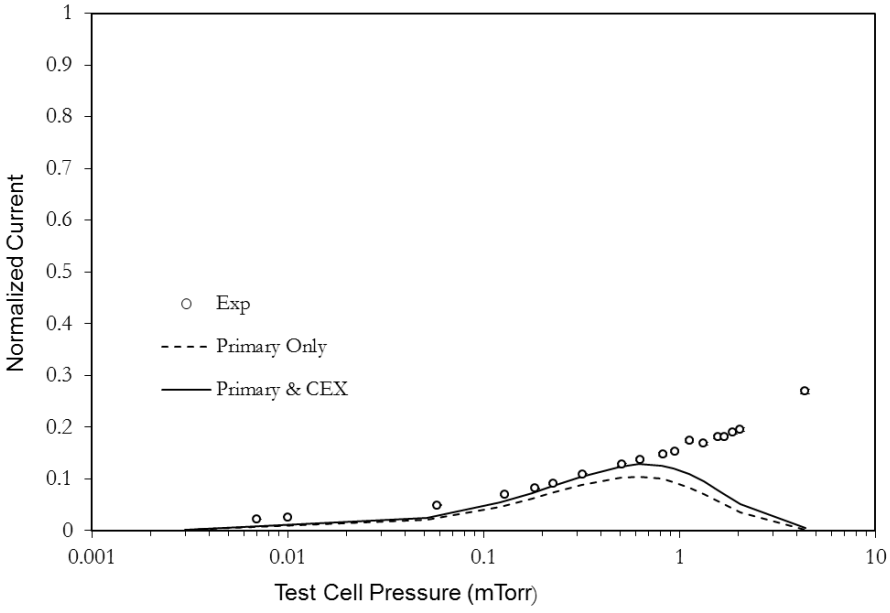

Figure 11. Comparison of experimental and computational results for current collected at the Exit Plate.

Referring to Figure 12, the majority of the current to the Inner Cylinder is due to CEX ions. These CEX ions are created by the primary ion collisions with background neutral gas. Due to the relatively high surface area of the Inner Cylinder, it is expected that the CEX ions created by these collisions are collected on this surface. However, the code does not predict the decrease in Inner Cylinder current at higher pressures as seen in the experiment. This discrepancy is similar to and opposite from that for the Exit Plate at higher pressures.

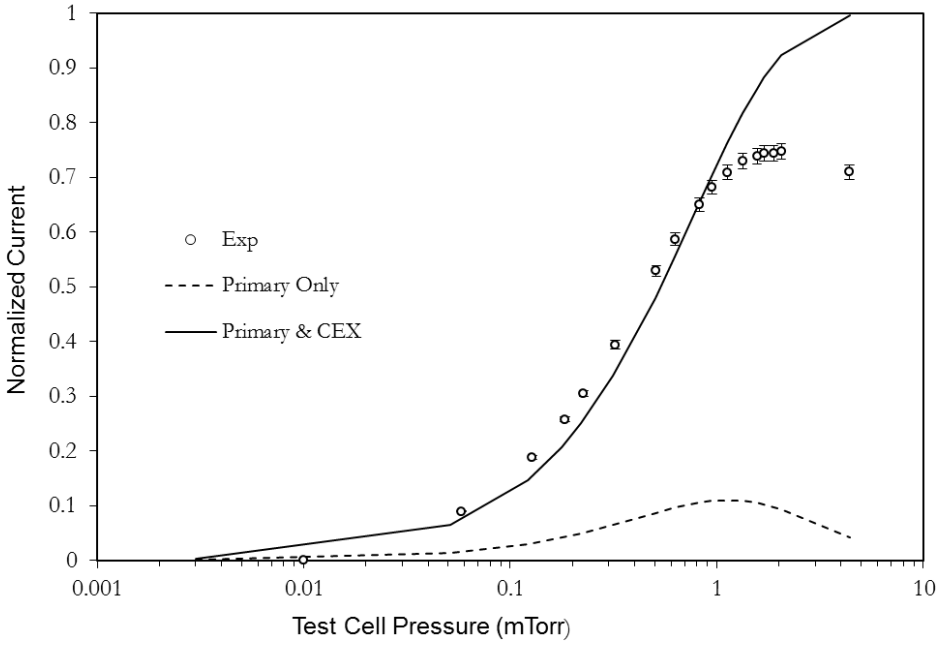

Figure 12. Comparison of experimental and computational results for current collected at the Inner Cylinder.

Comparing Figure 11 and Figure 12, the computational model predicts the behavior well until about 0.5 mTorr, beyond which the mean free path is less than the Test Cell length. It is apparent that agreement between the experiment and computational model is strong for one collision, but begins to deviate at higher pressures where multiple collisions are likely. As discussed in reference 5, in the case of large angle scattering, the energy of the incident ion can be reduced significantly. However, the scattering technique used in the model is a good approximation at high energies and not necessarily at lower energies[13]. Also, the model uses the same deflection function for the elastic and CEX collisions; however this assumption may not be appropriate and may lead to some of the disparity in the results[5].

The model is also capable of simulating the effect of secondary electron emission (SEE) due to the impact of heavy species on surfaces. Some preliminary results given in reference 5 suggest that secondary electrons may explain some of the disagreement; however, some additional information on the SEE behavior of the electrode surfaces used for the experiment is needed to further investigate these effects.

IV. Conclusions and Future Work

Detailed results have been obtained and reported for a simple and well-defined ion beam experiment. These data may be used for the development and validation of heavy species interactions for computational models. The "Test Cell" provides a simple domain that can be easily simulated by computational models[4,5]. Two different data sets

show good repeatability of the results for the Test Cell domain; however, measurements downstream of the cell suggest that the beam from Data Set 2 may have greater divergence. Comparison with a simple analytical relationship and computational results show that beam depletion due to ion-neutral collisions behaves as expected. Comparison with computational results for scattered and CEX ions shows that most of the ions collected on the Inner Cylinder of the Test Cell are due to CEX collisions. The computational and experimental results agree well at lower pressures that are below where the ion mean free path is equivalent to the Test Cell length. At higher pressures, the computational and experimental results do not agree well. This disagreement may be due to the way the computational model handles ion scattering, especially for multiple collisions for a single ion.

The experiment described herein provides useful results; however, there are several modifications to the experiment that will help provide better results for computational validation and development efforts. First of all, low SEE carbon material should be used for all electrode surfaces or materials with well-defined SEE behavior at the energies used in this experiment. Segmented electrodes can be used to provide greater spatial resolution of the Test Cell, including an electrode placed at the upstream surface of the Test Cell. Additional beam scan locations upstream of the Test Cell will give a better idea of the beam shape that enters the cell and the divergence of the beam. Additional tests using electrode biasing will soon be conducted to assess the effects of secondary electrons and CEX ions. Later efforts will focus on electrons and their interactions with heavy species.

Acknowledgements

The authors would like to thank the great technical and facility support that we have received from Lee Johnson and David Conroy of the Jet Propulsion Laboratory, California Institute of Technology. This work was supported by the University of California, Los Angeles (UCLA) School of Engineering and Applied Sciences and the Air Force Office of Scientific Research (AFOSR).

References

[1] Koo J. W., Boyd I. D., "Computational model of a Hall thruster," Computer Physics Communications 164 (2004) 442–447, doi: 10.1016/j.cpc.2004.06.058.

[2] Blahovec J. D., Bowers L. A., Luginsland J. W., Sasser G. E., Watrous J. J., "3-D ICEPIC Simulations of the Relativistic Klystron Oscillator," IEEE Transactions of Plasma Science, VOL. 28, NO. 3, JUNE 2000.

[3] Greenwood A. D., "An ICEPIC Convergence Study Using a Relativistic Magnetron," AFRL Technical Memorandum, AFRL-DE-PS-TM-2005-1005.

[4] Giuliano P. N., Boyd I. A., "Effects of detailed charge exchange interactions in DSMC-PIC simulation of a simplified plasma test cell," IEPC-2011-112, 32nd International Electric Propulsion Conference, Wiesbaden, Germany, Sept. 11-15, 2011.

[5] Araki S. J., Wirz R. E., "Collision Modeling for High Velocity Ions in a Quiescent Gas," AIAA-2011-3740, AIAA Plasmadynamics and Lasers Conference, Honolulu, Hawaii, June 26-30, 2011.

[6] Miller J. S., Pullins S. H., Levandier D. J., Chiu Y.-H., Dressler R. A., "Xenon charge exchange cross sections for electrostatic thruster models," Journal of Applied Physics, Vol. 91, No. 3, 2002, pp. 984-991.

[7] Bohm D., "The Characteristics of Electric Discharges in Magnetic Fields," (Guthrie A., Wakerling R.) pp. 1-76, 1949.

[8] Fossum E. C., King L. B., "Confinement time in an electron trap used for electron-mobility studies in Hall thruster-like fields," IEPC-2007-153.

[9] Matsubara A., Tanikawa T., "Anomalous Cross-Field Transport of Electrons Driven by the Electron-Ion Hybrid Instability Due to the Velocity Shear in a Magnetized Filamentary Plasma," Jpn. J. Appl. Phys. Vol. 39 (2000) pp. 4920-4932.

[10] Chiu Y.-H., Dressler R. a., Levandier D. J., Houchins C., Ng C. Y., "Large-angle xenon ion scattering in Xe-propelled electrostatic thrusters: differential cross sections," Journal of Physics D: Applied Physics, Vol. 41, No. 16, Aug. 2008.

[11] Fisher B., Krämer M., "Experimental Study of Drift Wave Turbulence and Anomalous Transport," Plasma Physics and Controlled Fusion, Vol. 31, No. 3, pp. 453-470, 1989.

[12] Massey H. S. W., Smith R. A., "The Passage of Positive Ions through Gases," *Proc. R. Soc. Lond. A* 1933 142, 142-172, doi: 10.1098/rspa.1933.0161.

[13] Mikellides I., Katz I., Kuharski R., and Mandell M., "Elastic Scattering of Ions in Electrostatic Thruster Plumes," Journal of Propulsion and Power, Vol. 21, No. 1, Jan. 2005, pp. 111-118.